

Article

# Dark Matter Sterile Neutrino from Scalar Decays

Lucia Aurelia Popa 

Institute of Space Science, Ro-077125 Magurele, Ilfov, Romania; lpopa@spacescience.ro

**Abstract:** We place constraints on DM sterile neutrino scalar decay production (SDP) assuming that sterile neutrinos represent a fraction from the total Cold Dark Matter energy density. For the cosmological analysis we complement the CMB anisotropy measurements with CMB lensing gravitational potential measurements, that are sensitive to the DM distribution to high redshifts and with the cosmic shear data that constrain the gravitational potential at lower redshifts than CMB. We also use the most recent low-redshift BAO measurements that are insensitive to the non-linear effects, providing robust geometrical tests. We show that our datasets have enough sensitivity to constrain the sterile neutrino mass  $m_{\nu_s}$  and the mass fraction  $f_s$  inside the co-moving free-streaming horizon. We find that the best fit value  $m_{\nu_s} = 7.88 \pm 0.73$  keV (68% CL) is in the parameter space of interest for DM sterile neutrino decay interpretation of the 3.5 keV X-ray line and that  $f_s = 0.86 \pm 0.07$  (68% CL) is in agreement with the upper limit constraint on  $f_s$  from the X-ray non-detection and Ly- $\alpha$  forest measurements that rejects  $f_s = 1$  at  $3\sigma$ . However, we expect that the future BAO and weak lensing surveys, such as EUCLID, will provide much more robust constraints.

**Keywords:** cosmic microwave background; dark matter; dark energy; cosmological observations



**Citation:** Popa, L.A. Dark Matter Sterile Neutrino from Scalar Decays. *Universe* **2021**, *7*, 309. <https://doi.org/10.3390/universe7080309>

Academic Editor: Norma G. Sanchez

Received: 25 June 2021

Accepted: 18 August 2021

Published: 21 August 2021

**Publisher's Note:** MDPI stays neutral with regard to jurisdictional claims in published maps and institutional affiliations.



**Copyright:** © 2021 by the author. Licensee MDPI, Basel, Switzerland. This article is an open access article distributed under the terms and conditions of the Creative Commons Attribution (CC BY) license (<https://creativecommons.org/licenses/by/4.0/>).

## 1. Introduction

The Cosmic Microwave Background (CMB) measurements from the PLANCK satellite, alone or in combination with other astrophysical datasets, provide no powerful evidence supporting new physics beyond the standard  $\Lambda$ CDM cosmological model [1,2]. With around 5% of the total energy density of the universe representing the baryonic matter, 21% the Dark Matter (DM) and 74% accounting for the Dark Energy (DE), the  $\Lambda$ CDM model is remarkably successful in reproducing the large-scale structure (LSS) of the universe. In addition, the Planck results show that the signature of the neutrino sector is consistent with the  $\Lambda$ CDM model assumptions and that DE is compatible with the  $\Lambda$  cosmological constant.

The nature and composition of DM is still unknown. Attempts involving collision-less DM particles fail to solve the  $\Lambda$ CDM problems in reproducing the cosmological structures at small scales (missing satellite problem [3–5], core-cusp problem [6–8], too-big-to-fail problem [9]), suggesting that DM particles may also exhibit gravitational properties and requiring the extension of the Standard Model (SM) of particle physics [10–12].

One of the theoretically well-motivated DM candidate is the sterile neutrino [13–15]. Arising in the minimal extension of SM, the sterile neutrino with mass in keV range can simultaneously explain the active neutrino oscillations, the DM properties and the matter–antimatter asymmetry of the universe [16,17].

Few independent detections of a weak X-ray emission line at an energy of  $\sim 3.5$  keV have been found in a stacked XMM-Newton spectrum of 73 galaxy clusters with redshifts in the range 0.01–0.35, in Chandra ACIS-I and ACIS-S spectra of Perseus [18] and in the XMM-Newton spectra of the Andromeda galaxy and the Perseus galaxy cluster [19]. Evidences of this emission have been also searched in the Milky Way with data from XMM-Newton [20,21] and Chandra [22], in deep Suzaku X-ray spectra of the central regions of Perseus, Coma, Virgo and Ophiuchus clusters [23,24], in the stacked XMM-Newton spectra of dwarf spheroidal galaxies in the vicinity of the Milky Way [25] and in the stacked spectra of a sample of galaxies selected from Chandra and XMM-Newton public archives [26]. The

origin of this line related either to a signature of decaying DM sterile neutrino with a mass of 7.1 keV [20] or to any known atomic transition in thermal plasma (with special interest in Potassium and Chlorine atomic transitions) [27] raised several controversies [28]. The evidence of this emission line in different astrophysical sites is expected to place strong constraints on both hypotheses.

Several keV sterile neutrino DM production mechanisms have been proposed.

In the Dodelson–Widrow (DW) scenario [29], keV sterile neutrinos are produced by non-resonant oscillations with active neutrinos in presence of negligible leptonic asymmetry. This mechanism is now excluded by the observations of structure formation as it produces too hot sterile neutrino velocity spectra [30,31].

The keV sterile neutrino DM resonant production (RP) via the conversion of active to sterile neutrinos through the Shi–Fuller mechanism in presence of leptonic asymmetry [32] has also been investigated [33]. In this scenario, sterile neutrino parameters required to reproduce the X-ray line of  $\sim 3.5$  keV are consistent with the main cosmological parameters inferred from present cosmological measurements, Local Group and high- $z$  galaxy count constraints [33]. However, some tension with Ly- $\alpha$  data still exists [34].

The keV sterile neutrino DM production by particle decays has been also extensively discussed (see [35] and references therein). A particularly interesting case is the DM sterile neutrino production by scalar decay (SDP). This process involves a generic scalar singlet with the vacuum expectation value (VEV) that could be produced via SM Higgs interactions. Depending on the strength of the Higgs coupling  $\lambda_H$ , the singlet scalar can be produced like Weakly Interacting Massive Particles (WIMPs) via freeze-out [15,36] or like “Feeble Interacting Massive Particles” (FIMPs) via freeze-in mechanisms and must couple with the right-handed neutrino fields through the Yukawa interaction, leading to sterile neutrino Majorana masses [34,37]. A complete treatment of the SDP mechanism for the whole parameter space, giving the general solution at the level of momentum distributions is presented in [38].

So far, the keV sterile neutrino DM properties have been addressed by evaluating their impact on the co-moving free streaming horizon, that relates to the average of sterile neutrino velocity distribution. However, for such models characterised by a highly non-thermal momentum distribution, the average momentum is subject to uncertainties, leading to a fail of the free-streaming horizon in constraining the sterile neutrino parameters [34]. The existing constraints are, in general, obtained in linear theory under the assumption that sterile neutrinos are all DM [37,39].

The aim of this paper is to place constraints on the properties of DM sterile neutrinos produced by the SDP mechanism through their impact on distance–redshift relations and the growth of structures. We consider models where DM is a mixture of CDM and DM sterile neutrinos and analyse if the existing measurements of the CMB gravitational potential, the baryon acoustic oscillation (BAO) and the weak gravitational lensing of galaxies can constrain DM sterile neutrinos properties.

The paper is organized as follows: Section 2 summarizes the SDP Boltzmann formalism calculations. Section 3 describes the model parameters and the methods involved in the analysis. Section 4 presents the datasets. In Section 5 we present our results and discuss the cosmological implications of the sterile neutrino SDP mechanism. The conclusions are summarised in Section 6.

## 2. Sterile Neutrino Production by the Scalar Decay (SDP)

In this section, we present the sterile neutrino SDP calculations.

The evolution of momentum distributions for scalar,  $f_S$ , and sterile neutrino,  $f_{\nu_s}$ , are obtained by solving the coupled Boltzmann equations:

$$\hat{L}[f_S] = C^S, \quad \hat{L}[f_{\nu_s}] = C^{\nu_s}, \quad (1)$$

where  $\mathcal{C}^S$  and  $\mathcal{C}^{\nu_s}$  are scalar and sterile neutrino collision terms encoding the effects of different processes that contribute to their production and  $\hat{L}$  is the Liouville operator:

$$\hat{L} = \frac{\partial}{\partial t} - \mathcal{H}p \frac{\partial}{\partial p}. \tag{2}$$

In the above equation,  $p$  is the particle momentum and  $\mathcal{H}$  is the Hubble expansion rate. Equation (1) can be written in a more convenient form by performing the following variable transformations [38]:

$$\begin{aligned} t &\rightarrow r = r(t, p), \\ p &\rightarrow \zeta = \zeta(t, p). \end{aligned} \tag{3}$$

Exploiting the correspondence between temperature  $T$  and time  $t$  and by using the conservation of the co-moving entropy, the above transformations can be written in the form (for details see Appendix A.2 in [38]):

$$\begin{aligned} r &= \frac{m_0}{T}, \\ \zeta &= \left( \frac{g_s(T_0)}{g_s(T)} \right)^{1/3} q, \end{aligned} \tag{4}$$

where  $q = p/T$  is the co-moving momentum and  $g_s(T)$  is the effective number of entropy degrees of freedom. We choose  $m_0 = T_0 = m_h$  where  $m_h = 125$  GeV is the Higgs boson mass. In terms of the new variables, the Liouville operator reads as:

$$\hat{L} = \mathcal{H}r \left( \frac{Tg'_s(T)}{3g_s(T)} + 1 \right)^{-1} \frac{\partial}{\partial r}, \tag{5}$$

where  $'$  denotes the derivative with respect to the temperature.

The time–temperature relation is obtained as:

$$\frac{dT}{dt} = -\mathcal{H}T \left( \frac{Tg'_s(T)}{3g_s(T)} + 1 \right)^{-1}. \tag{6}$$

Equation (6) assumes the conservation of the co-moving entropy density:

$$\frac{2\pi}{45} g_s(T) T^3 a^3 = \text{const.} = s_0, \tag{7}$$

where  $a$  is the cosmological scale factor ( $a_0 = 1$  today) and  $s_0 = 2891.2 \text{ cm}^{-3}$  is the present entropy density. We used the fitting formulas from [40] to compute the evolution of the effective number of the entropy degrees of freedom  $g_s(T)$  and its derivative  $g'_s(T)$ .

In this work, we take the leading processes contributing to the collision terms  $\mathcal{C}^S$  and  $\mathcal{C}^{\nu_s}$  from Equation (1) of the form:

$$\begin{aligned} \mathcal{C}^S &= \mathcal{C}_{hh \leftrightarrow SS}^S + \mathcal{C}_{S \rightarrow \nu_s \nu_s}^S \\ \mathcal{C}^{\nu_s} &= \mathcal{C}_{S \rightarrow \nu_s \nu_s}^{\nu_s} \end{aligned} \tag{8}$$

where:  $\mathcal{C}_{hh \leftrightarrow SS}^S$  describes the depletion of scalars due to the annihilation into pairs of SM Higgs particles and the reverse process,  $\mathcal{C}_{S \rightarrow \nu_s \nu_s}^S$  describes the decay of scalars into pairs of sterile neutrinos and  $\mathcal{C}_{S \rightarrow \nu_s \nu_s}^{\nu_s}$  describes the creation of sterile neutrinos from the decays of scalars. With these assumptions, the SDP scenario is parameterized with respect to the sterile neutrino mass  $m_{\nu_s}$ , the scalar mass  $M_S$ , the strength of the Higgs coupling  $\lambda_H$  and of the Yukawa coupling  $y_k$ .

Using the explicit forms of the collision terms given in [38], we simultaneously evolve the Equations (1) and (6) to obtain the scalar and sterile neutrino momentum distributions in the expanding universe.

Figure 1 presents the dependence of the sterile neutrino final momentum distribution obtained for a given scalar mass  $M_S$  and different values of  $\lambda_H$  and  $y_k$ .

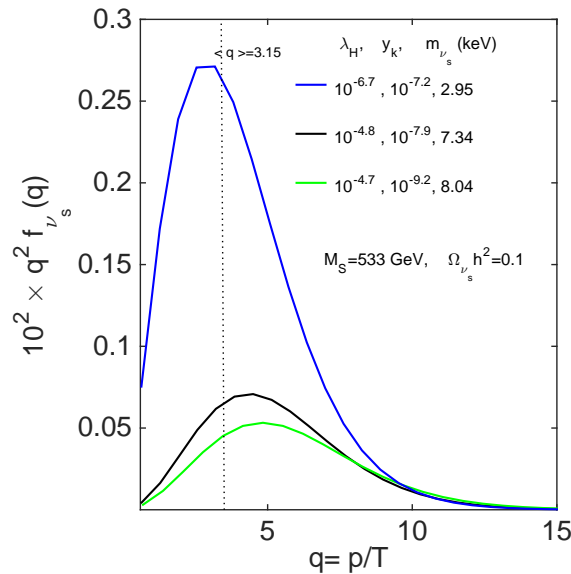


**Figure 1.** The dependence of the sterile neutrino momentum distributions on the co-moving momentum  $q = p/T$  for the scalar mass  $M_S = 533$  GeV and different values of the Higgs coupling,  $\lambda_H$ , and Yukawa coupling,  $y_k$ . The dotted line indicates the averaged co-moving momentum corresponding to sterile neutrino thermal distribution. Other parameters are fixed to:  $\Omega_b h^2 = 0.0226$ ,  $\Omega_c h^2 = 0.112$ ,  $\Omega_\nu h^2 = 0.00064$ ,  $H_0 = 70$  km s<sup>-1</sup>Mpc<sup>-1</sup>.

The sterile neutrino number density  $n_{\nu_s}(r)$  and the physical energy density  $\Omega_{\nu_s} h^2$  are then given by:

$$n_{\nu_s}(r) = \frac{N}{2\pi^2} \frac{g_s(T)}{g_s(T_0)} \left(\frac{m_0}{r}\right)^3 \int_0^\xi d\xi \xi^2 f_{\nu_s}(\xi, r), \tag{9}$$

$$\Omega_{\nu_s} h^2 = \frac{s_0}{s(r)} \frac{m_{\nu_s} n_{\nu_s}(r)}{\rho_c/h^2}, \tag{10}$$

where  $s(r)$  is the co-moving entropy density and  $\rho_c/h^2 = 1.054 \cdot 10^{-2}$  MeV cm<sup>-3</sup> is the critical density in terms of reduced Hubble constant  $h$ .

Figure 2 presents the dependence of the abundances of scalar and sterile neutrino on the time parameter  $r = m_h/T$  for the same models presented in Figure 1.

We test the production code over a large parameter space and find that our distributions are in agreement with similar distributions obtained in [37,38].

The SDP mechanism relies on the assumption that the Higgs boson, that is sourcing the scalar production, is in thermal equilibrium. To assess the validity of this assumption, we evaluate the total time available for the Higgs boson to decouple from the thermal plasma. Since DM production happens in the early Universe, we consider the era of radiation dominance.

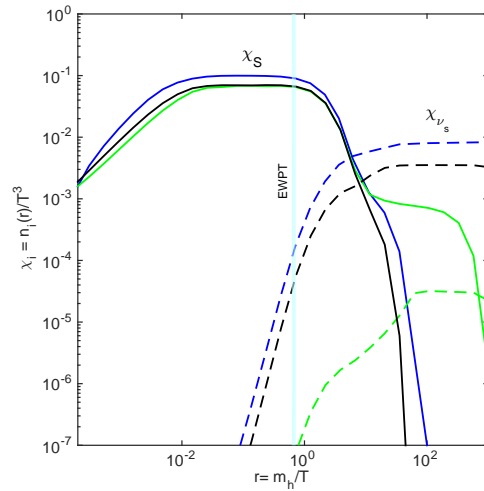


**Figure 2.** The dependence of the abundances of scalar (continuous lines) and sterile neutrino (dashed lines) on the time parameter  $r = m_h/T$  for the same models presented in Figure 1. The vertical blue line indicates the temperature of the electroweak phase transition (EWPT).

During this epoch, the Hubble time is  $t(T) \sim M_0/2T^2$  where  $T$  is the plasma temperature and  $M_0$  is a function that depends on  $T$  via the evolution of the number of entropy degrees of freedom  $g_s(T)$ :  $M_0(T) = 7.35 g_s^{-1/2}(T) \times 10^{18}$  GeV [36]. We evaluate  $t(T)$  assuming that the Higgs boson decouples from the thermal plasma at a temperature similar to its mass, namely  $T_h \sim 125$  GeV. Assuming  $g_s(T_h) = 106.5$ , we find  $t(T_h) \sim 1.51 \times 10^{-11}$  s. The Higgs vacuum lifetime is  $\tau_h \sim 1.56 \times 10^{-22}$  s [41]. During the Higgs lifetime, the scalars are generated through  $hh \rightarrow SS$  annihilation process. Then, the reverse process  $SS \rightarrow hh$  generates Higgs particles in thermal equilibrium if the scalar lifetime  $\tau_S = 16\pi/(y_t^2 m_S)$  is smaller than the time available for the Higgs boson to decouple from the thermal plasma. Through these processes, the Higgs boson population is kept constant and in thermal equilibrium. For example, for the pair  $(m_S, y_t) = (533 \text{ GeV}, 10^{-7.2})$  we obtain  $\tau_S = 1.4 \times 10^{-11}$  s, while for  $(m_S, y_t) = (60 \text{ GeV}, 10^{-6})$  we obtain  $\tau_S = 5.5 \times 10^{-13}$  s. In both cases, the Higgs boson is in equilibrium sourcing the scalar production.

After the scalar develops a non-zero VEV, the DM sterile neutrinos can be produced through the decay  $S \rightarrow \nu_s \nu_s$ , leading to sterile neutrino masses  $m_{\nu_s} = y_k \langle S \rangle$ , where  $\langle S \rangle$  is the scalar VEV. The collision term  $C^{\nu_s}$  in Equation (8) is controlled by the scalar effective decay width function  $C_\Gamma = M_0(T)y_t/m_S^2$  [37].

The production of sterile neutrinos occurs mainly at temperatures on the order of the scalar mass,  $T_{prod} \sim 10^2$  GeV. The reduction in the effective number of degrees of freedom from  $g_*(T_{prod}) = 106.5$  to  $g_*(0.1 \text{ MeV}) = 3.36$  and the entropy production that takes place as the universe cools from  $T_{prod}$  causes the DM sterile neutrino population to be diluted and redshifted. Following [36], these processes dilute the population of sterile neutrinos by a factor  $\xi \geq 33$  in the density and by a factor  $\xi^{1/3} \geq 3.2$  in the average momentum for the SM degrees of freedom, leading to DM sterile neutrinos cold enough to satisfy the bounds on small-scale structures. Such sterile neutrinos can decay into neutrinos and photons with energy  $E_\gamma = m_{\nu_s}/2$ , reaching the sensitivity of X-ray observatories.

### 3. Parameterization and Methods

The baseline model is an extension of the flat  $\Lambda$ CDM model, described by the following cosmological parameters:

$$\mathbf{P}_{\Lambda\text{CDM}} = \left\{ \Omega_b h^2, \Omega_c h^2, \theta_s, \tau, \log(10^{10} A_s), n_s, \sum m_\nu, N_{eff} \right\},$$

where:  $\Omega_b h^2$  is the present baryon energy density,  $\Omega_c h^2$  is the present CDM energy density,  $\theta_s$  is the ratio of sound horizon to angular diameter distance at decoupling,  $\tau$  is the optical

depth at reionization,  $A_s$  and  $n_s$  are amplitude and spectral index of primordial power spectrum of curvature perturbations at pivot scale  $k = 0.05 \text{ Mpc}^{-1}$ ,  $\sum m_\nu$  is the total mass of three active neutrino flavors and  $N_{eff}$  the number of relativistic degrees of freedom that parameterize the contributions from non-interacting relativistic particles. In the SM with three active neutrino flavours,  $N_{eff} = 3.046$  due to non-instantaneous decoupling corrections [42].

The SDP model extends the baseline model by including the following parameters:

$$\mathbf{P}_{SDP} = \{m_{\nu_s}, M_S, y_k, \lambda_H\},$$

where:  $m_{\nu_s}$  is the sterile neutrino mass,  $M_S$  is the scalar mass,  $y_k$  is the Yukawa strengths coupling and  $\lambda_H$  the Higgs strengths coupling. The sterile neutrino mass fraction is a derived parameter,  $f_S = \Omega_{\nu_s}/\Omega_c$ , where the sterile neutrino energy density  $\Omega_{\nu_s}$  is computed using Equation (10). The matter energy density is then given by  $\Omega_m = \Omega_c + \Omega_b + \Omega_\nu + \Omega_{\nu_s}$ .

We modify the Boltzmann code camb<sup>1</sup> [43] to allow the calculation of sterile neutrino SDP formalism presented in the previous section.

The parameter extraction from cosmological datasets is based on the Monte-Carlo Markov Chain (MCMC) technique. We modify the publicly available version of the package CosmoMC<sup>2</sup> [44] to sample from the space of cosmological and sterile neutrino SDP mechanism parameters and generate estimates of their posterior mean and confidence intervals. We first run the modified versions of CosmoMC and camb setting to zero the additional parameters of the SDP model. We find good consistency between our bounds and the existing constraints for the  $\Lambda$ CDM model [1]. We use the default convergence settings implemented in CosmoMC: MPI\_Limit\_Converge = 0.025 and MPI\_Limit\_Converge\_Err = 0.2. With these choices, the CosmoMC run stops when the confidence interval for each parameter at 95% C.L. is accurate at  $0.2\sigma$ . This error can be reduced, but in this case the computing time increases to reach the convergence limit. This is critical for non-standard models as SDP for which the execution time is larger than in the standard case because of numerical evolution of momentum distributions in camb. The final runs are based on 120 independent channels, reaching the convergence criterion  $(R - 1) = 0.007$ , defined as the ratio between the variance of the means and the mean of variances for the second half of chains [44].

We assume a flat Universe and uniform priors for all parameters adopted in the analysis in the intervals listed in Tables 1 and 2.

The Hubble expansion rate  $H_0$  and sterile neutrino energy density  $\Omega_{\nu_s}h^2$  are derived parameters in our analysis. We constrained  $H_0$  values to reject the extreme models and restrict the values of  $\Omega_{\nu_s}h^2$  to the interval of  $\Omega_c h^2$ .

The sterile neutrino lower mass limit is restricted by the universal Tremaine–Gunn bound [45] valid for the case in which all DM is made by sterile neutrinos.

A stronger bound is coming from the analysis of DM phase-space distribution in dwarf spheroidal galaxies, leading to  $m_{\nu_s} > 1.8 \text{ keV}$  for the sterile neutrino non-resonant production (NRP) [46]. This bound was revisited in [47] for the  $\Lambda$  Cold plus Warm Dark Matter model ( $\Lambda$ CWDM) where WDM in the form of sterile neutrinos is a fraction  $f_{WDM}$  from the total DM. For  $f_{WDM} = 1$  (pure  $\Lambda$ WDM model), the combined analysis of WMAP5 and Ly- $\alpha$  datasets led to a lower bound on sterile neutrino mass  $m_{\nu_s} > 1.6 \text{ keV}$  (at 95%CL) in the NRP case. The same analysis shows that after a certain value of the lower bound of sterile neutrino mass  $f_{WDM}$  approaches a constant value because the contribution of the WDM component becomes too small to be constrained by the data.

We made MCMC convergence tests with different priors on the parameters of SDP models leading to  $m_{\nu_s} = 2 \text{ keV}$  as the smallest mass of sterile neutrino included in the present analysis. The upper bound value of the sterile neutrino mass is restricted by the non-detection of the emission lines from X-ray observations [48].

**Table 1.** Priors and constraints for the  $\Lambda$ CDM-ext parameters adopted in the analysis. All priors are uniform in the listed intervals. We assume a flat Universe.

Parameter	Prior
$\Omega_b h^2$	[0.005, 0.1]
$\Omega_c h^2$	[0.001, 0.5]
$100\theta_s$	[0.5, 10]
$\tau$	[0.01, 0.9]
$\log(10^{10} A_s)$	[2.5, 5]
$n_s$	[0.5, 1.5]
$m_\nu$ (eV)	[0, 6]
$N_{eff}$	[3.046, 8]
$H_0$ (km s <sup>-1</sup> Mpc <sup>-1</sup> )	[20, 100]

**Table 2.** Priors and constraints on the additional parameters for SDP models. All priors are uniform in the listed intervals.

SDP Parameter	Prior
$m_{\nu_s}$ (keV)	[2, 30]
$y_k$	[10 <sup>-10</sup> , 10 <sup>-8</sup> ]
$\lambda_H$	[10 <sup>-8</sup> , 10 <sup>-4</sup> ]
$M_S$ (GeV)	[10, 1000]
$\Omega_{\nu_s} h^2$	[0.001, 0.5]

#### 4. Cosmological Datasets

For the cosmological analysis, we use the following datasets:

**The CMB measurements:** We use the CMB angular power spectra from the PLANCK experiment [1] and the PLANCK likelihood codes corresponding to different multipole ranges: Commander for  $2 \leq l \leq 29$ , CamSpec  $50 \leq l \leq 2500$ , LowLike for  $2 \leq l \leq 32$  for polarization data and Lensing for  $40 \leq l \leq 400$  for lensing data. As sterile neutrino production is expected to affect the redshift–distance relations and the growth of structures, we include in the analysis the PLANCK power spectrum of the reconstructed lensing potential [2]. We will refer to the combination of these measurements as the PLANCK+lens dataset.

**The baryonic acoustic oscillations (BAO):** BAO measurements are low-redshift probes insensitive to non-linear effects because their characteristic acoustic scale, of around 147 Mpc, is much larger than the scale of the virialized cosmological structures. Moreover, as BAO features in the matter power spectrum can be observed as a function of both angular and redshift separations [49,50], these measurements are robust geometrical tests. We include in the analysis the BAO characteristic parameter measurements from the Baryon Oscillation Spectroscopic Survey (BOSS) LOWZ at  $z_{eff} = 0.32$ , CMASS at  $z_{eff} = 0.57$  [50] and 6dF Galaxy Survey (6dFGS) at  $z_{eff} = 0.1$  [51]. We will refer to the combination of these measurements as the BAO dataset.

**Cosmic shear:** Weak lensing of galaxies, or cosmic shear, probes the gravitational potential at redshifts lower than the CMB lensing. We use the COSMOMC implementation of the one-year Dark Energy Survey (DES) cosmic shear measurements described in [52], referred hereafter as DES dataset.

#### 5. Analysis and Results

##### 5.1. Sensitivity of Cosmological Data to $m_{\nu_s}$ and $f_S$

A change in sterile neutrino mass fraction  $f_S$  leads first to a change in the Hubble expansion rate  $H$ . At the CMB photons decoupling ( $T_{cmb} = 0.26$  eV), the changes in  $H$  lead to changes in the sound horizon distance  $r_s$  (that scales as  $1/H$ ) and in the photon diffusion damping  $r_d$  (that scales as  $\sqrt{1/H}$ ).

The CMB anisotropy spectrum is sensitive to both  $r_s$  and  $r_d$  changes as projected angles over the co-moving angular distance,  $D_A$ , to the last scattering:  $\theta_s = r_s/D_A$  and  $\theta_d = r_d/D_A$ . While a change in  $\theta_s$  shifts the position of the acoustic Doppler peaks through the CMB anisotropy spectrum, a change in  $\theta_d$  relative to  $\theta_s$  modifies its amplitude. CMB can measure the expansion rate by measuring the ratio  $\theta_d/\theta_s \sim \sqrt{H}$ .

For models sharing the same value of  $f_s$ , the ratio  $\theta_d/\theta_s$  is a measure of the relativistic energy density at  $T_{\text{cmb}}$ , usually parameterized by  $N_{\text{eff}}(T_{\text{cmb}})$  [53]. The contribution of sterile neutrinos to  $N_{\text{eff}}(T_{\text{cmb}})$  encodes information on their mass and production mechanism parameters that lies in the momentum distribution function and can be computed by comparing the sterile neutrino kinetic energy density to the energy density of other relativistic particles in equilibrium at  $T_{\text{cmb}}$  [37].

The BAO measurements lead to joint constraints on the co-moving angular diameter distance,  $D_A(z)$ , and on the Hubble parameter,  $H(z)$ , at smaller redshifts than CMB. At these redshifts, for models sharing the same sterile neutrino mass fraction, both  $D_A(z)$  and  $H(z)$  are degenerated. The BAO observations typically constrain the quantity  $r_s(z_d)/D_V(z)$ ,  $r_s(z_d)$  is the sound horizon distance at the drag epoch redshift  $z_d$  and  $D_V(z)$  is given by:

$$D_V(z) = \left[ (1+z)^2 D_A^2(z) \frac{cz}{H(z)} \right]^{1/3}, \tag{11}$$

where  $c$  is the speed of light.

Figure 3 presents the redshift dependence of the variation  $\Delta(r_s(z_d)/D_V(z))$  for models sharing the same  $f_s$  obtained in the SDP scenario, showing that the BAO measurements break the degeneracy between these models, leading to constraints on sterile neutrino mass and production parameters.

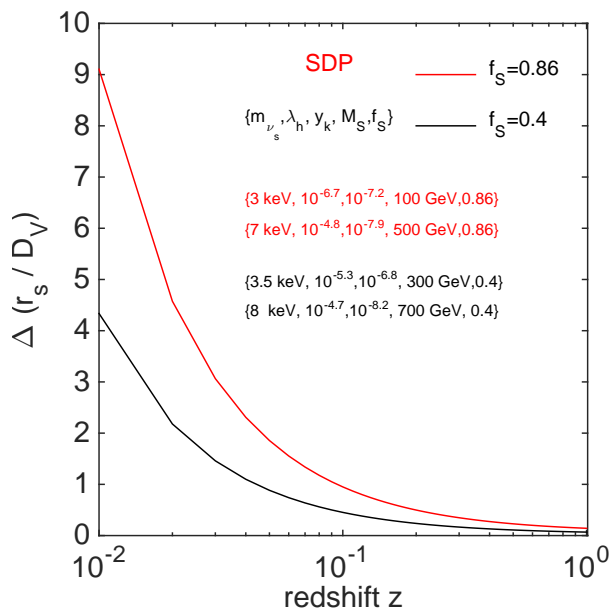


**Figure 3.** Redshift dependence of the variation of BAO characteristic parameter,  $\Delta(r_s(z_d)/D_V(z))$ , for models sharing the same sterile neutrino mass fraction  $f_s$  in the SDP scenario. The production mechanism parameters are indicated for each case. Other parameters are fixed to:  $\Omega_b h^2 = 0.0226$ ,  $\Omega_c h^2 = 0.112$ ,  $\Omega_\nu h^2 = 0.00064$ ,  $H_0 = 70 \text{ km s}^{-1} \text{Mpc}^{-1}$ .

The gravitational lensing of the CMB photons provides direct measurements on scales where the effects of sterile neutrino are expected to manifest. The largest scale affected is the present value of the co-moving free-streaming horizon given by [47]:

$$\lambda_{fsh}^0 = \int_{T_0}^{T_{\text{prod}}} \frac{\langle v(T) \rangle}{a(T)} \frac{dt}{dT} dT, \tag{12}$$

where  $\langle v(T) \rangle$  is the velocity dispersion of sterile neutrinos,  $T_{prod}$  is the sterile neutrino production temperature and  $T_0$  is the present temperature. We compute  $\lambda_{fsh}^0$  following the analytical approach from [47]:

$$\lambda_{fsh}^0 = \frac{a_{nr}}{\sqrt{\Omega_R} H_0} \left( 1 + 6 \text{Arcsinh} \sqrt{\frac{a_{eq}}{a_{nr}}} \right), \tag{13}$$

where  $a_{eq} = \Omega_R/\Omega_m$  is the scale factor at matter–radiation equality,  $a_{nr} = T_0/m_{\nu_s}$  is the scale factor at the time of sterile neutrino non-relativistic transition,  $\Omega_R$  is the radiation energy density and  $\Omega_m$  is the matter energy density. The analytical approach assumes that the Universe is completely radiation-dominated until  $a_{eq}$  and neglects the small contribution to the integral (12) from dark energy. We account for the entropy dilution from  $T_{prod}$  until  $T_0$  rescaling  $\lambda_{fsh}^0$  by a factor  $\bar{\zeta}_s^{1/3} = g_s(T_{prod})/g_s(T_0)$  [34], where  $g_s$  is the effective number of relativistic entropy degrees of freedom ( $g_s(T_{EWFT}) \approx 109.5$  and  $g_s(T_0) \approx 3.36$ ).

Figure 4 presents the likelihood probability distributions of the free-streaming horizon wave-number  $k_{fs}^{min}$ , obtained for our models. One should note that these wave-numbers,  $k \sim 1 \text{ hMpc}^{-1}$ , correspond to the typical size of dwarf galaxies [37], while the observations of Ly- $\alpha$  absorption in spectra of distant quasars are tracers of linear density fluctuations on scales  $0.1 < k < 3 \text{ hMpc}^{-1}$ .

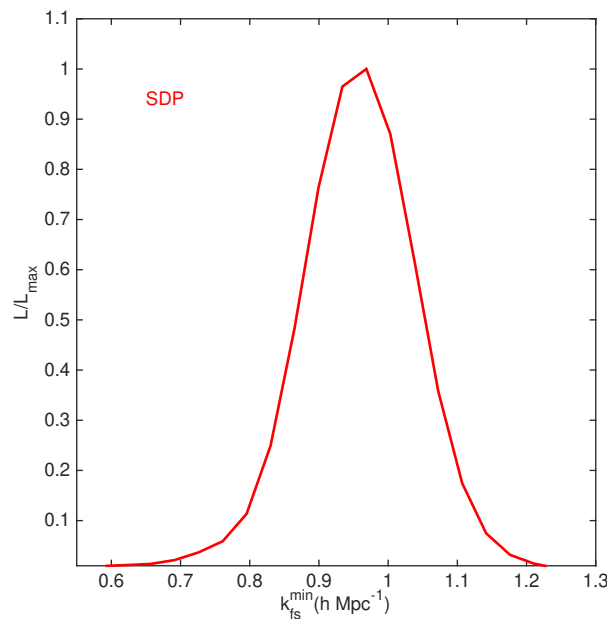


**Figure 4.** The likelihood probability distribution of the estimated free-streaming horizon wave-number,  $k_{fs}^{min}$ , from the fit of SDP models with PLANCK + lens + BAO + DES datasets.

On the other hand, the power spectrum of the CMB-projected gravitational potential,  $C_l^{\phi\phi}$ , is sensitive to both geometry and growth of structures. In the Limber approximation,  $C_l^{\phi\phi}$  can be written as:

$$C_l^{\phi\phi} = \frac{8\pi}{l^3} \int_0^{\chi^*} d\chi D_A(\chi) \left( \frac{D_A(\chi^*) - D_A(\chi)}{D_A(\chi^*) D_A(\chi)} \right)^2 P_{\Psi}(z(\chi), k = l/D_A(\chi)), \tag{14}$$

where:  $\chi$  is the co-moving coordinate distance,  $\chi^*$  is the co-moving coordinate distance to the last scattering surface,  $k$  is the wave-number,  $D_A(\chi)$  is the co-moving angular diameter distance and  $P_{\Psi}(z, k)$  is the power spectrum of the gravitational potential.

Figure 5 presents the deflection angle power spectra obtained for models sharing the same values of  $f_S$  and  $m_{\nu_s}$ . We indicate the contributions of different wave-numbers  $k$  (in  $\text{Mpc}^{-1}$ ) to the deflection angle power spectra. The figure shows that for the multipole range involved in this analysis,  $40 \leq l \leq 400$ , the deflection angle power spectrum of the CMB lensing potential is sensitive to the DM sterile neutrino parameters.

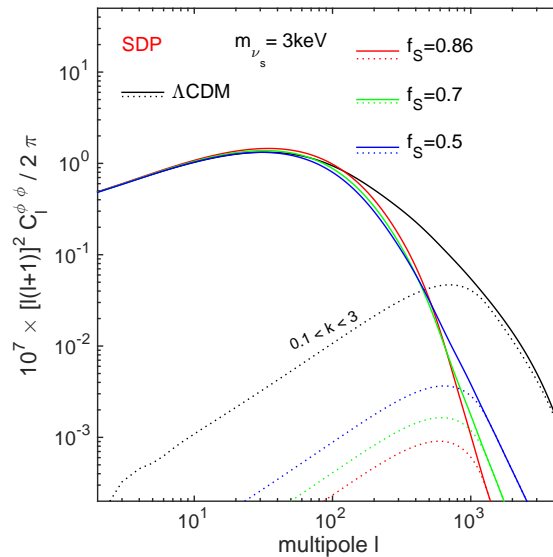


**Figure 5.** The dependence of the deflection angle power spectra on sterile neutrino mass fraction  $f_S$  in models sharing the same sterile neutrino mass  $m_{\nu_s}$ , obtained in the SDP scenario. For comparison, we plot the deflection angle power spectrum for the  $\Lambda\text{CDM}$  model. The contributions of the wave-numbers in the range  $0.1 < k < 3 \text{ Mpc}^{-1}$  are also indicated (dotted lines). Other parameters are fixed to:  $\Omega_b h^2 = 0.0226$ ,  $\Omega_c h^2 = 0.112$ ,  $\Omega_\nu h^2 = 0.00064$ ,  $H_0 = 70 \text{ km s}^{-1} \text{ Mpc}^{-1}$ .

We conclude that PLANCK + lens + BAO + DES datasets have enough sensitivity to constrain the sterile neutrino mass and mass fraction inside the co-moving free-streaming horizon.

## 5.2. Cosmological Constraints

Table 3 presents the mean values and the absolute errors of the main cosmological parameters from the fit of  $\Lambda\text{CDM-ext}$  and SDP models with the PLANCK + lens + BAO + DES datasets. We found a good agreement of the cosmological predictions for all cosmological parameters within  $1-\sigma$ .

Constraints on several cosmological parameters are highly dependent on the number of priors and cosmological datasets. As we do not include the high- $l$  CMB polarization data in the analysis, we find a higher value for  $\tau$  than that obtained by the PLANCK Collaboration [1].

Our datasets probe scales where the effects of sterile neutrino are expected to manifest. Moreover, the damped amplitude of the CMB anisotropy at small scales, quantified by  $e^{-2\tau}$ , is accurately constrained by the CMB lensing power spectra, while the lensing potential reconstruction provides the determination of the amplitude independent on the optical depth. As the CMB lensing power spectrum constrains the matter density fluctuations along the line of sight, the present-day *rms* matter density power,  $\sigma_8$ , is also determined. On the other hand, the CMB small-scale anisotropy directly fixes the combination  $\sigma_8 e^{-\tau}$  that is tightly constrained by the CMB data. We find a very good consistency between the values of  $\sigma_8 e^{-\tau} = 0.741 \pm 0.021$  (68% CL) obtained from our analysis and  $\sigma_8 e^{-\tau} = 0.768 \pm 0.009$  (68% CL) obtained from the analysis of PLANCK CMB data alone, in the case of the  $\Lambda\text{CDM}$  model.

The values of other cosmological parameters presented in Table 3 for the  $\Lambda$ CDM model are in good agreement with the PLANCK Collaboration results obtained from the joint analysis of the CMB-lensing, BAO and galaxy-lensing (see Table 2 in [2]).

Figure 6 shows the likelihood probability distributions and the joint confidence regions obtained for the SDP mechanism parameters.

The dominant effect on DM sterile neutrino production is given by the strength of the Higgs coupling  $\lambda_H$ , that sets the scalar mass at  $M_S \simeq 533 \pm 47$  GeV and the strength of Yukawa coupling  $y_k$  sets the sterile neutrino mass at  $m_{\nu_s} = 7.88 \pm 0.73$  keV, leading to sterile neutrino DM mass fraction  $f_S = 0.86 \pm 0.07$  (errors at 68% C.L.). This value clearly indicates that a dominant component of DM can be produced by the SDP mechanism.

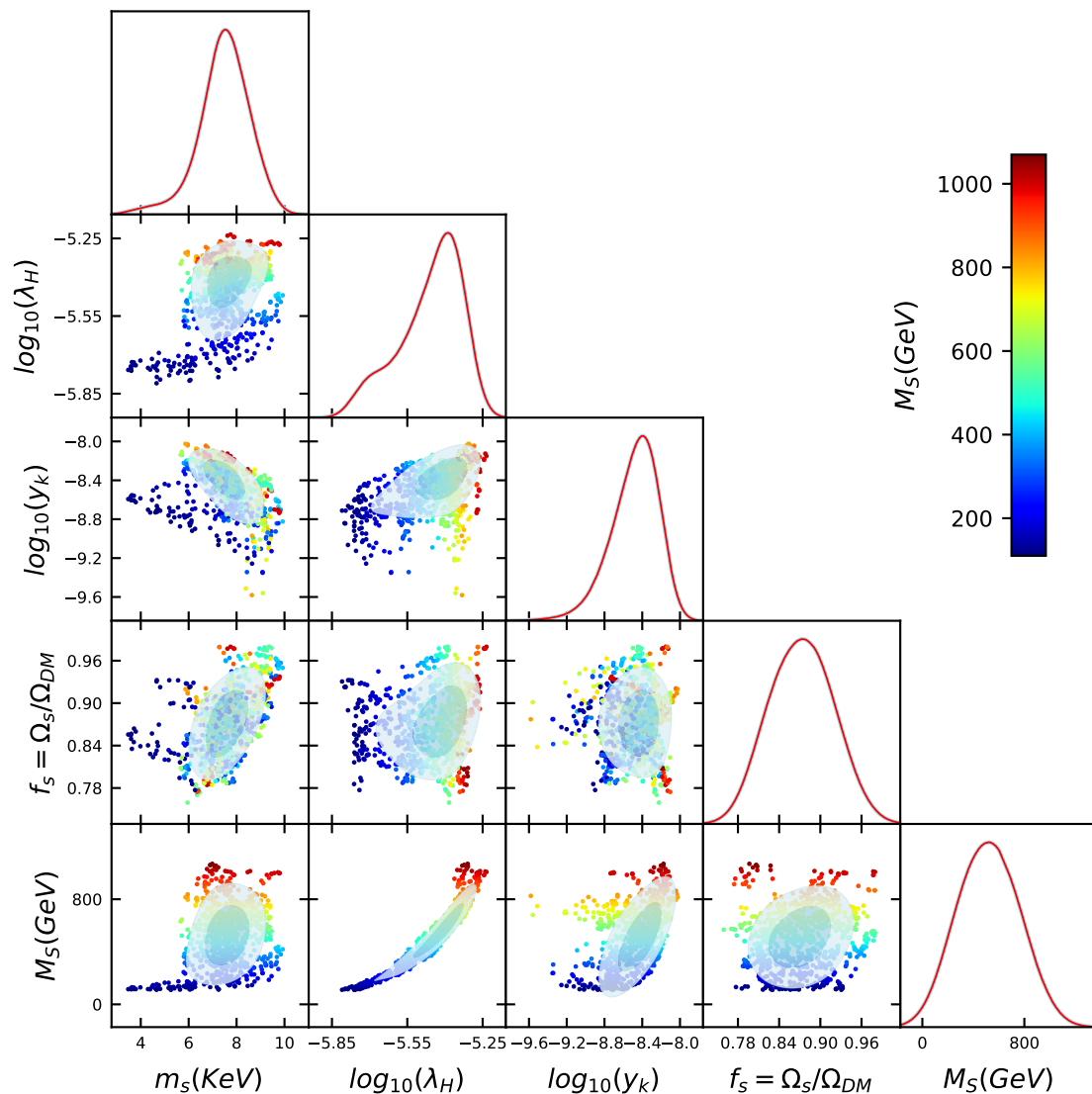


**Figure 6.** The marginalized likelihood probability distributions and the joint confidence regions (68% and 95% CL) for SDP mechanism parameters color-coded by the scalar mass values  $M_S$ . The dominant effect on SDP mechanism is given by the strength of the Higgs coupling,  $\lambda_H$ , that sets  $M_S$ , and the strength of Yukawa coupling,  $y_k$ , that sets  $m_{\nu_s}$ . The best fit values of the SDP parameters lead to  $f_S = 0.86 \pm 0.07$  (68% C.L.), indicating that SDP is a dominant mechanism.

**Table 3.** The mean values and the absolute errors of the main parameters obtained from the fit of  $\Lambda$ CDM-ext and SDP models with the PLANCK + lensing + BAO + DES datasets. The errors are quoted at 68% C.L. The upper limits are quoted at 95% C.L. The first group of parameters are the base cosmological parameters sampled in the Monte-Carlo Markov Chain analysis with uniform priors. The others are derived parameters.

Parameter	$\Lambda$ CDM-Ext	SDP
$\Omega_b h^2$	$0.0223 \pm 0.0002$	$0.0219 \pm 0.0003$
$\Omega_c h^2$	$0.122 \pm 0.004$	$0.121 \pm 0.004$
$100\theta_{MC}$	$1.0412 \pm 0.0008$	$1.0413 \pm 0.0009$
$\tau$	$0.087 \pm 0.015$	$0.069 \pm 0.012$
$\sum m_\nu$	$<0.321$	$<0.198$
$N_{eff}$	$3.520 \pm 0.259$	$3.380 \pm 0.243$
$f_S$		$0.860 \pm 0.071$
$M_S$ (GeV)		$533.60 \pm 47.21$
$10^{-6} \lambda_H$		$3.780 \pm 0.642$
$10^{-9} y_k$		$3.451 \pm 1.820$
$\Omega_m$	$0.295 \pm 0.013$	$0.284 \pm 0.011$
$\sigma_8$	$0.808 \pm 0.021$	$0.832 \pm 0.019$
$\sigma_8(\Omega_m/0.3)^{0.5}$	$0.801 \pm 0.004$	$0.809 \pm 0.005$
$\sigma_8 e^{-\tau}$	$0.741 \pm 0.021$	$0.776 \pm 0.018$
$H_0$	$70.512 \pm 1.556$	$71.210 \pm 1.433$
$m_{\nu_s}$ (keV)		$7.882 \pm 0.731$

### 6. Conclusions

We place constraints on the DM sterile neutrino produced by the scalar decay (SDP), assuming that sterile neutrino represents a fraction  $f_S$  from the total CDM energy density. So far, the keV sterile neutrino properties have been addressed under the assumption that sterile neutrinos are all DM, by evaluating their impact on the co-moving free streaming horizon that relates on the average velocity distribution.

For such models, characterized by highly non-thermal momentum distributions, the average momentum is subject to uncertainties and the free-streaming horizon fails to constrain the DM sterile neutrino parameters.

For our cosmological analysis, we complement the CMB anisotropy data with the CMB lensing gravitational potential measurements, that are sensitive to the DM distribution to high redshifts and with the cosmic shear data, that constrain the gravitational potential at lower redshifts than the CMB anisotropy.

We also use the most recent low-redshift BAO measurements that are insensitive to the non-linear effects, providing robust geometrical tests.

We show that for models sharing the same DM sterile neutrino mass fraction  $f_S$ , the accurate determination of the acoustic scale from CMB anisotropy measurements breaks the degeneracy of Hubble parameter at the photon decoupling, constraining the sterile neutrino mass  $m_{\nu_s}$ , while the BAO measurements constrain  $m_{\nu_s}$  at lower redshifts. We evaluate the co-moving free-streaming horizon showing that the deflection angle power spectrum of the CMB lensing potential,  $C_l^{\phi\phi}$ , is sensitive to sterile neutrino production mechanism parameters for the multipole range involved in this analysis ( $40 \leq l \leq 400$ ). Depending on both the angular diameter distance and the matter density fluctuations, we show that  $C_l^{\phi\phi}$  can break the degeneracy between sterile neutrino mass  $m_{\nu_s}$  and mass fraction  $f_S$ . We also show that our datasets have enough sensitivity to constrain  $m_{\nu_s}$  and  $f_S$  inside the co-moving free-streaming horizon.

We find that the best fit values of  $m_{\nu_s}$  are in the parameter space of interest for sterile neutrino DM decay interpretation of the 3.5 keV X-ray line [19] and the DM sterile neutrino mass fraction is  $f_S = 0.86 \pm 0.07$  (at 68% CL), in agreement with the upper limit constraint on  $f_S$  from the X-ray non-detection and Ly- $\alpha$  forest measurements that rejects  $f_S = 1$  at  $3\sigma$

level [48]. We expect that the future BAO and weak lensing surveys, such as EUCLID, will provide much more robust constraints on the DM sterile neutrino properties.

**Funding:** This research received no external funding.

**Institutional Review Board Statement:** Not applicable.

**Informed Consent Statement:** Not applicable.

**Data Availability Statement:** Not applicable.

**Acknowledgments:** The author acknowledges the use of the GRID system computing facility at the Institute of Space Science developed under UEFSCDI contract 18PCCDI/2018 and ESA/Prodex contract 4000124902.

**Conflicts of Interest:** The author declares no conflict of interest.

## Notes

<sup>1</sup> <http://camb.info>, CAMB v.1.1.2 accessed on 31 May 2020.

<sup>2</sup> <http://cosmologist.info>, accessed on 31 May 2020.

## References

1. Aghanim, N.; Akrami, Y.; Ashdown, M.; Aumont, J.; Baccigalupi, C.; Ballardini, M.; Banday, A.J.; Barreiro, R.B.; Bartolo, N.; Basak, S.; et al. Planck 2018 results VI. Cosmological parameters. *Astron. Astrophys.* **2020**, *641*, A6.
2. Aghanim, N.; Akrami, Y.; Ashdown, M.; Aumont, J.; Baccigalupi, C.; Ballardini, M.; Banday, A.J.; Barreiro, R.B.; Bartolo, N.; Basak, S.; et al. Planck 2018 results VIII. Gravitational lensing. *Astron. Astrophys.* **2020**, *641*, A8.
3. Klypin, A.; Kravtsov, A.V.; Valenzuela, O.; Prada, F. Where Are the Missing Galactic Satellites? *Astrophys. J.* **1999**, *522*, 82. [[CrossRef](#)]
4. Zwaan, M.A.; Meyer, M.J.; Staveley-Smith, L. The velocity function of gas-rich galaxies. *Mon. Not. R. Astron. Soc.* **2010**, *403*, 1969. [[CrossRef](#)]
5. Papastergis, E.; Martin, A.M.; Giovanelli, R.; Haynes, M.P. The Velocity Width Function of Galaxies from the 40% ALFALFA Survey: Shedding Light on the Cold Dark Matter Overabundance Problem. *Astrophys. J.* **2010**, *739*, 38. [[CrossRef](#)]
6. Salucci, P.; Burkert, A. Dark Matter Scaling Relations. *Astrophys. J.* **2000**, *737*, 9. [[CrossRef](#)]
7. Gentile, G.; Salucci, P.; Klein, U.; Vergani, D.; Kalberla, P. The cored distribution of dark matter in spiral galaxies. *Mon. Not. R. Astron. Soc.* **2004**, *351*, 903. [[CrossRef](#)]
8. de Naray, R.K.; Kaufmann, T. Recovering cores and cusps in dark matter haloes using mock velocity field observations. *Mon. Not. R. Astron. Soc.* **2011**, *414*, 3617. [[CrossRef](#)]
9. Boylan-Kolchin, M.; Bullock, J.S.; Kaplinghat, M. Too big to fail? The puzzling darkness of massive Milky Way subhaloes. *Mon. Not. R. Astron. Soc.* **2011**, *415*, L40. [[CrossRef](#)]
10. Jungman, G.; Kamionkowski, M.; Griest, K. Supersymmetric dark matter. *Phys. Rep.* **1996**, *267*, 195. [[CrossRef](#)]
11. Bertone, G.; Hooper, D.; Silk, J. Particle dark matter: Evidence, candidates and constraints. *Phys. Rep.* **2005**, *405*, 279. [[CrossRef](#)]
12. Feng, J.L. Dark Matter Candidates from Particle Physics and Methods of Detection. *Ann. Rev. Astron. Astrophys.* **2010**, *48*, 495. [[CrossRef](#)]
13. Abazajian, K.N.; Fuller, G.M.; Patel, M. Sterile neutrino hot, warm and cold dark matter. *Phys. Rev. D* **2001**, *64*, 023501. [[CrossRef](#)]
14. Boyarsky, A.; Ruchayskiy, O.; Shaposhnikov, M. The Role of sterile neutrinos in cosmology and astrophysics. *Ann. Rev. Nucl. Part. Sci.* **2009**, *59*, 191. [[CrossRef](#)]
15. Kusenko, A. Sterile neutrinos: The Dark side of the light fermions. *Phys. Rep.* **2009**, *481*, 1. [[CrossRef](#)]
16. Asaka, T.; Blanchet, S.; Shaposhnikov, M. The MSW dark matter and neutrino masses. *Phys. Lett. B* **2005**, *631*, 151. [[CrossRef](#)]
17. Asaka, T.; Shaposhnikov, M. The MSM, dark matter and baryon asymmetry of the universe. *Phys. Lett. B* **2005**, *620*, 17. [[CrossRef](#)]
18. Bulbul, E.; Markevitch, M.; Foster, A.R.; Smith, R.K.; Loewenstein, M.; Randall, S.W. Detection of An unidentified emission line in the Stacked X-ray spectrum of Galaxy Clusters. *Astrophys. J.* **2014**, *789*, 13. [[CrossRef](#)]
19. Boyarsky, A.; Ruchayskiy, O.; Iakubovskiy, D.; Franse, J. Unidentified Line in X-Ray Spectra of the Andromeda Galaxy and Perseus Galaxy Cluster. *Phys. Rev. Lett.* **2014**, *113*, 251301. [[CrossRef](#)]
20. Boyarsky, A.; Franse, J.; Iakubovskiy, D.; Ruchayskiy, O. Checking the dark matter origin of 3.53 keV line with the Milky Way centre. *Phys. Rev. Lett.* **2015**, *115*, 161301. [[CrossRef](#)]
21. Jeltema, T.E.; Profumo, S. Discovery of a 3.5 keV line in the Galactic Centre and a critical look at the origin of the line across astronomical targets. *Mon. Not. R. Astron. Soc.* **2015**, *450*, 2143. [[CrossRef](#)]
22. Riemer-Sørensen, S. Constraints on the presence of a 3.5 keV dark matter emission line from Chandra observations of the Galactic centre. *Astron. Astrophys.* **2016**, *590*, A71. [[CrossRef](#)]
23. Loewenstein, M.; Kusenko, A.; Biermann, P.L. New Limits on Sterile Neutrinos from Suzaku Observations of the Ursa Minor Dwarf Spheroidal Galaxy. *Astrophys. J.* **2009**, *700*, 426.

24. Urban, O.; Werner, N.; Allen, S.W.; Simionescu, A.; Kaastra, J.S.; Strigari, L.E. A Suzaku Search for Dark Matter Emission Lines in the X-ray Brightest Galaxy Clusters. *Mon. Not. R. Astron. Soc.* **2015**, *451*, 2447–2261. [[CrossRef](#)]
25. Malyshev, D.; Neronov, A.; Eckert, D. Constraints on 3.55 keV line emission from stacked observations of dwarf spheroidal galaxies. *Phys. Rev. D* **2014**, *90*, 1035062014 [[CrossRef](#)]
26. Anderson, M.E.; Churazov, E.; Bregman, J.N. Non-Detection of X-Ray Emission From Sterile Neutrinos in Stacked Galaxy Spectra. *Mon. Not. R. Astron. Soc.* **2015**, *452*, 3905–3923. [[CrossRef](#)]
27. Bulbul, E.; Markevitch, M.; Foster, A.; Smith, R.K.; Loewenstein, M. Comment on “Dark matter searches going bananas: the contribution of Potassium (and Chlorine) to the 3.5 keV line”. *arXiv* **2014**, arXiv:1409.4143.
28. Carlson, E.; Jeltema, T.; Profumo, S. Where do the 3:5 keV photons come from? A morphological study of the Galactic Center and of Perseus. *J. Cosmol. Astropart. Phys.* **2015**, *2*, 9. [[CrossRef](#)]
29. Dodelson, S.; Widrow, L.M. Sterile-neutrinos as dark matter. *Phys. Rev. Lett.* **1994**, *72*, 17. [[CrossRef](#)]
30. Canetti, L.; Drewes, M.; Frossard, T.; Shaposhnikov, M. Dark matter, baryogenesis and neutrino oscillations from right-handed neutrinos. *Phys. Rev. D* **2013**, *87*, 093006 [[CrossRef](#)]
31. Merle, A.; Niro, V. Influence of a keV sterile neutrino on neutrinoless double beta decay: How things changed in recent years. *Phys. Rev. D* **2013**, *88*, 113004 [[CrossRef](#)]
32. Shi, X.D.; Fuller, G.M. A New dark matter candidate: Nonthermal sterile neutrinos. *Phys. Rev. Lett.* **1999**, *82*, 2832. [[CrossRef](#)]
33. Laine, M.; Shaposhnikov, M. Sterile neutrino dark matter as a consequence of MSM-induced lepton asymmetry. *J. Cosmol. Astropart. Phys.* **2008**, *6*, 31 [[CrossRef](#)]
34. Merle, A.; Schneider, A. Production of Sterile Neutrino dark matter and the 3.5 keV line. *Phys. Lett. B* **2015**, *749*, 283–288. [[CrossRef](#)]
35. Adhikari, R.; Agostini, M.; Ky, N.A.; Araki, T.; Archidiacono, M.; Bahr, M.; Baur, J.; Behrens, J.; Bezrukov, F.; Dev, P.B.; et al. A White Paper on keV sterile neutrino Dark Matter. *J. Cosmol. Astropart. Phys.* **2017**, *1*, 25. [[CrossRef](#)]
36. Petraki, K.; Kusenko, A. Dark-matter sterile neutrinos in models with a gauge singlet in the Higgs sector. *Phys. Rev. D* **2008**, *77*, 065014. [[CrossRef](#)]
37. Merle, A.; Totzauer, M. keV Sterile Neutrino Dark Matter from Singlet Scalar Decays: Basic Concepts and Subtle Features. *J. Cosmol. Astropart. Phys.* **2015**, *1506*, 11. [[CrossRef](#)]
38. König, J.; Merle, A.; Totzauer, M. keV sterile neutrino dark matter from singlet scalar decays: The most general case. *J. Cosmol. Astropart. Phys.* **2016**, *11*, 38. [[CrossRef](#)]
39. Murgia, R.; Merle, A.; Viel, M.; Totzauer, M.; Schneider, A. Non-cold dark matter at small scales: A general approach. *J. Cosmol. Astropart. Phys.* **2017**, *11*, 46 [[CrossRef](#)]
40. Wantz, O.; Shellard, E.P.S. Axion Cosmology Revisited. *Phys. Rev. D* **2010**, *82*, 123508. [[CrossRef](#)]
41. Zyla, P.A.; Barnett, R.M.; Beringer, J.; Dahl, O.; Dwyer, D.A.; Groom, D.E.; Lin, C.J.; Lugovsky, K.S.; Pianori, E.; Robinson, D.J.; et al. Review of Particle Physics. *Prog. Theor. Exp. Phys.* **2020**, *8*, 083C01. [[CrossRef](#)]
42. Mangano, G.; Miele, G.; Pastor, S.; Pinto, T.; Pisanti, O.; Serpico, P.D. Relic neutrino decoupling including flavour oscillations. *Nucl. Phys. B* **2005**, *729*, 221. [[CrossRef](#)]
43. Lewis, A.; Challinor, A.; Lasenby, A. Efficient computation of CMB anisotropies in closed FRW models. *Astrophys. J.* **2000**, *538*, 473. [[CrossRef](#)]
44. Lewis, A.; Bridle, S. Cosmological parameters from CMB and other data: A Monte Carlo approach. *Phys. Rev. D* **2002**, *66*, 103511. [[CrossRef](#)]
45. Tremaine, S.; Gunn, J.E. Dynamical role of light neutral leptons in cosmology. *Phys. Rev. Lett.* **1979**, *42*, 407. [[CrossRef](#)]
46. Boyarsky, A.; Ruchayskiy, O.; Iakubovskiy, D. A lower bound on the mass of dark matter particles. *J. Cosmol. Astropart. Phys.* **2009**, *3*, 5. [[CrossRef](#)]
47. Boyarsky, A.; Lesgourgues, J.; Ruchayskiy, O.; Viel, M. Lyman- $\alpha$  constraints on warm and on warm-plus-cold dark matter models. *J. Cosmol. Astropart. Phys.* **2009**, *905*, 12. [[CrossRef](#)]
48. Palazzo, A.; Cumberbatch, D.; Slosar, A.; Silk, J. Sterile neutrinos as subdominant warm dark matter. *Phys. Rev. D* **2007**, *76*, 103511. [[CrossRef](#)]
49. Anderson, L.; Aubourg, E.; Bailey, S.; Beutler, F.; Bhardwaj, V.; Blanton, M.; Bolton, A.S.; Brinkmann, J.; Brownstein, J.R.; Burden, A.; et al. The clustering of galaxies in the SDSS-III Baryon Oscillation Spectroscopic Survey: Baryon Acoustic Oscillations in the Data Release 10 and 11 galaxy samples. *Mon. Not. R. Astron. Soc.* **2014**, *441*, 24. [[CrossRef](#)]
50. Gil-Marín, H.; Percival, W.J.; Cuesta, A.J.; Brownstein, J.R.; Chuang, C.H.; Ho, S.; Kitaura, F.S.; Maraston, C.; Prada, F.; Rodríguez-Torres, S.; et al. The clustering of galaxies in the SDSS-III Baryon Oscillation Spectroscopic Survey: BAO measurement from the LOS-dependent power spectrum of DR12 BOSS galaxies. *Mon. Not. R. Astron. Soc.* **2016**, *460*, 4210. [[CrossRef](#)]
51. Beutler, F.; Blake, C.; Colless, M.; Jones, D.H.; Staveley-Smith, L.; Campbell, L.; Parker, Q.; Saunders, W.; Watson, F. The 6dF Galaxy Survey: Baryon Acoustic Oscillations and the Local Hubble Constant. *Mon. Not. R. Astron. Soc.* **2011**, *416*, 3017. [[CrossRef](#)]
52. Troxel, M.A.; MacCrann, N.; Zuntz, J.; Eifler, T.F.; Krause, E.; Dodelson, S.; Gruen, D.; Blazek, J.; Friedrich, O.; Samuroff, S.; et al. Dark Energy Survey Year 1 Results: Cosmological Constraints from Cosmic Shear. *Phys. Rev. D* **2018**, *D 98*, 043528. [[CrossRef](#)]
53. Hou, Z.; Keisler, R.; Knox, L.; Millea, M.; Reichardt, C. How massless neutrinos affect the cosmic microwave background damping tail. *Phys. Rev. D* **2013**, *87*, 083008 [[CrossRef](#)]